Electronic Supplementary Material (ESI) for RSC Advances.
This journal is © The Royal Society of Chemistry 2015

Complementarity of neutron reflectometry and ellipsometry for the study of atmospheric reactions at the air–water interface.

Federica Sebastiani[a,b], Richard A. Campbell[b*] and Christian Pfrang.[a*]

[a] *Department of Chemistry, University of Reading, P.O. Box 224, RG6 6AD, Reading, UK*

[b] *Institut Laue-Langevin, 71 avenue des Martyrs, CS20156, 38042 Grenoble Cedex 9, France*

* corresponding authors: campbell@ill.eu and c.pfrang@reading.ac.uk

Electronic Supporting Information

1. Neutron reflectometry: brief physical basis

Specular neutron reflectometry (NR) is a technique used to study the structure of materials normal to an interface. In particular, it is an accurate and direct method to determine the surface excess of an organic monolayer at the air–water interface.[1] In this case, the model commonly used to describe the experimental system is made up by a uniform layer with a refractive index different to those of the ambient phase and the subphase. The refractive index, n, of a material is given by[2]

$$n^2 \approx 1 - \frac{\rho\lambda^2}{\pi} \qquad (1)$$

where λ is the neutron wavelength, ρ is the scattering length density given by $\sum_i b_i N_i$, and b_i is the scattering length and N_i the number density of species i in the material. In most cases $\rho > 0$ hence $n < 1$; for reference $n_{\text{air}} = 1$. We are interested specifically in a deuterated monolayer at the air–liquid interface where the aqueous subphase is air contrast matched water (ACMW), which has $\rho = 0\ \text{Å}^{-2}$. In this case the intensity of the reflection is directly related to the presence of deuterated form of the molecule at the interface:

$$\text{R} \approx \frac{16\pi^2}{q^4}.4b^2N^2\sin^2\left(\frac{qd}{2}\right) \qquad (2)$$

where $q = \frac{4\pi\sin\theta}{\lambda}$ is the momentum transfer in Å^{-1}, θ is the angle of incidence and d is the thickness of the layer in Å. From eq. 2 it is apparent that the intensity of R at low q depends on ρ, and the modulation of R at higher values of q gives information on d. The chemical composition of the interface determines the value of b, and by appropriately fitting the $R(q)$ profile N can be obtained. Once, ρ and d are known, the surface excess, Γ, is given by:

$$\Gamma = \frac{\rho d}{b} \qquad (3)$$

By comparing eqs 2 and 3, it is found that $R \propto \Gamma^2$. A feature of Γ in the thin film limit is that it is insensitive to details of the applied optical matrix model, even if the values of ρ and d are model-dependent; in fact at very low q the two quantities vary inversely giving a roughly equivalent product.

2. Neutron reflectometry: raw data and analysis

The $\log_{10}R(q)$ profiles were obtained by a pre-treatment of the raw data from the 2-D detector. The time-of-flight detector image shows the number of neutrons reflected at a given reflection angle with respect to the wavelength. The reflectivity is the number of neutrons in the specular reflection, where the reflection angle equals the incident angle, divided by the number of incident neutrons on the sample for discrete narrow bands of wavelengths. This treatment was performed using the standard data reduction software COSMOS, a routine provided by the Institut Laue-Langevin (ILL, Grenoble, France) in the framework of LAMP.[3] The data were normalized relative to the total reflection of an air–D_2O sample below the critical edge.

Once all the reflectivity profiles were obtained, they were fitted with the Motofit routine which runs in IgorPro.[4] The program allows building an optical matrix model to simulate the reflectivity of a given interfacial structure or fit parameters using a weighted least-squares fitting procedure which affects the reflectivity of experimental data. The model used consists of a semi-infinite ambient phase (air) and a sub-phase (air contrast matched water, ACMW), and between them there is a single deuterated monolayer. The layer was described by a homogeneous scattering length density and thickness. Furthermore, the roughness values (σ) of the air–monolayer and monolayer–subphase interfaces and the background value were additional parameters. The scattering length density was fixed to 5.95×10^{-6} Å^{-2}, a value determined theoretically using the calculated the molecular volume with the procedure introduced by Armen *et al.* (1998).[5] The roughness of the air–monolayer and monolayer–water interfaces were both approximated to be constant at 3 Å, consistent with capillary wave theory[2,6] given that the surface tension was always > 65 mN m^{-1}. The background value for any given experiment was determined by measurements of the air–ACMW interface and was always in the range $2.5 – 3.5 \times 10^{-5}$. The thickness of a full dMO monolayer was determined using an NR measurement over a wider q-range (up to 0.25 Å^{-1}) and was found to be 16.1 ± 0.1 Å with a solvent penetration of 1.3 ± 0.1%. During the fitting of the reflectivity profiles measured during oxidation the values of thickness, the scattering length density and roughness were kept constant, while the solvent penetration was allowed to change (further details of this analysis may be found in Pfrang *et al.*, 2014).[7] A contribution for the inter-mixing of the reactant with possible products of limited duration in the monolayer is ignored on the basis that at the very low q values measured the effect of small changes to the roughness used has a negligible effect on the fitted surface excess. We fitted the reflectivity profile, fixing the thickness and using the scattering length density as a parameter; we thus obtained a value for the surface excess for each reflectivity profile using eq. 3. Figure S1 shows examples of measured neutron reflectivity profiles and the fitted curves. The profiles are for a complete and unreacted monolayer of dMO as well as for oxidized monolayers at intermediate and low coverages.

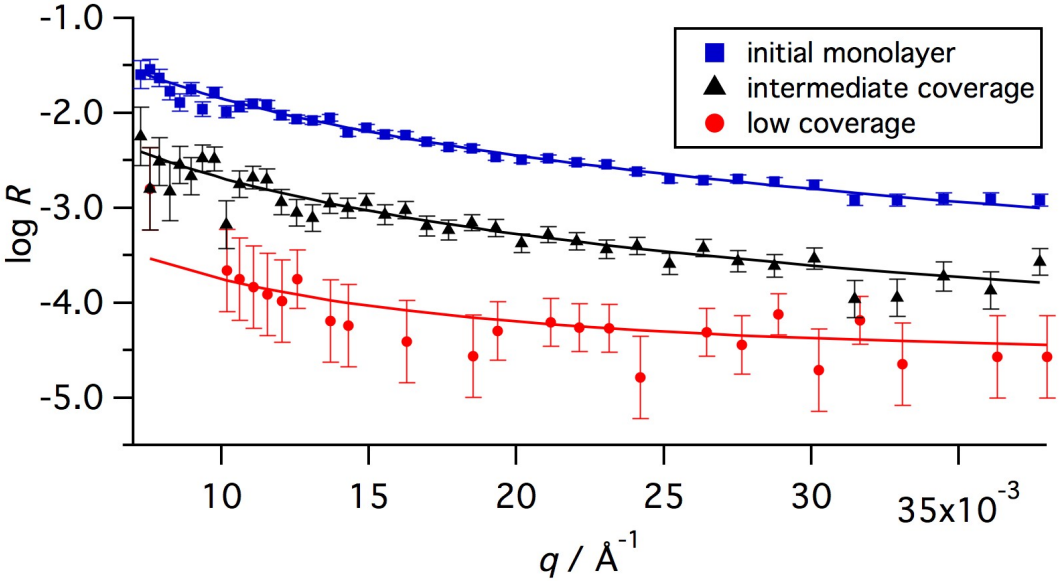

Figure S1: Examples of neutron reflectivity profiles recorded for a monolayer of dMO on ACMW for the initial, unreacted monolayer (blue squares), intermediate coverage (black triangles) and low coverage (red circles). The fits are illustrated by the solid lines. Parameters for the data presented: d = 16.1 ± 0.1 Å; ρ = 5.95 × 10^{-6} $Å^{-2}$; σ = 3 Å; solvent penetration was 0.8 ± 0.5%, 62 ± 1% and 90 ± 2% for initial, intermediate and low coverage, respectively; the background was 2.61 × 10^{-5} and the scattering length densities of air and ACMW were fixed to zero.

3. Ellipsometry: brief physical basis

The polarisation of light changes when it is reflected at an interface, *i.e.* light polarised perpendicular to the reflection plane (*s*-polarised) reflects differently from light polarised parallel to the plane (*p*-polarised). The relative amplitude and the phase of the *p*- and *s*-components vary by different amounts. The attenuation, Ψ, and the phase shift, Δ, depend on the optical properties of the surface and on the angle of incidence, θ_i. These values are related to the Fresnel reflectivity coefficients, r_p and r_s, parallel and perpendicular components respectively,[8]

$$\frac{r_p}{r_s} = \tan\Psi\, e^{i\Delta} \qquad (4)$$

Ellipsometry is widely used to study adsorption at solid–liquid and solid–gas interfaces, because of the large contrast due to different refractive indices of the components. For a transparent air–liquid interface a key limitation is that Ψ is very insensitive to the optical properties of thin films. Often the study of surface layers at the air–water interface is restricted to analysis of only the phase shift;[9,10] the exception being when the film thickness extends beyond ~ 10 nm when it is useful to analyze Ψ as well.[11] The greatest advantages of ellipsometry are its high sensitivity and its precision in the surface excess. The measurements can also be extremely fast (~ 10^{-2} s), although most instruments acquire data on timescales of a few seconds and the probed surface is very small (~ mm^2 compared to several cm^2 for NR). Ellipsometry is therefore a highly suitable technique to follow changes in the amount of surface material. This difference in probed surface area has the added advantage that fluctuations in the optical signal may be related to lateral domains of material present on the

micrometer to millimeter scale.[12,13] The presence of a surface monolayer at the air–water interface changes Δ relative to the value for the clean interface, Δ_{H_2O}.

4. Ellipsometry: raw data

Figure S2 shows examples of the optical phase shift, *i.e.* Δ with respect to Δ_{H_2O}, measured using ellipsometry prior to conversion to Γ for the oxidation of hMO monolayers by O_3.

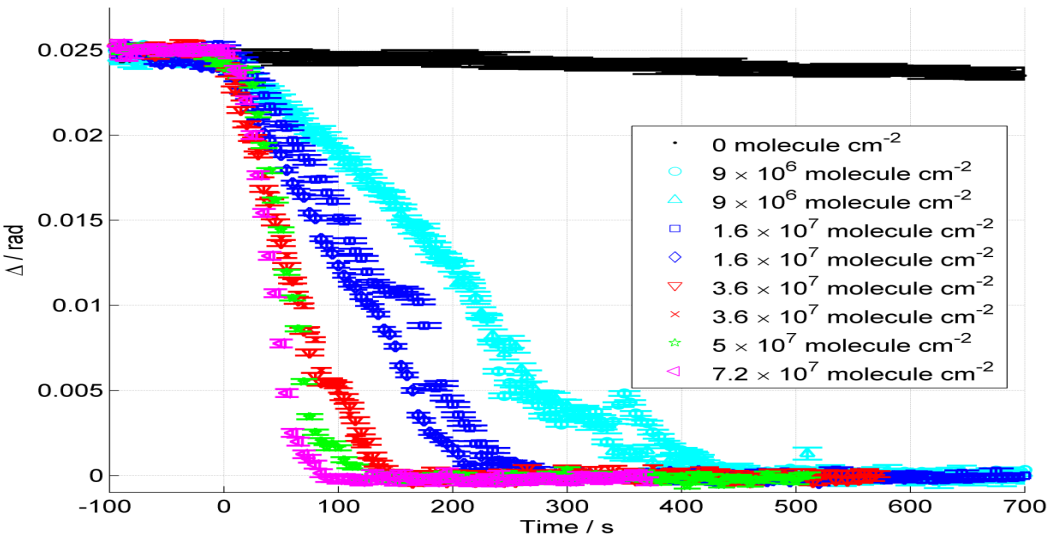

Figure S2: hMO monolayers exposed to ozone: Δ values obtained by ellipsometry as a function of time for different oxidant concentrations. Error bars correspond to one standard deviation.

5. Calibration of surface excess from ellipsometry

A calibration of Δ to Γ was carried out for methyl oleate monolayers at the air–water interface. This was achieved by spreading different known amounts of dMO in the carrier solvent chloroform on ACMW for NR or on pure H_2O for ellipsometry. Figure S3 shows the resulting calibration plot. While linear[13] and empirical quadratic[14] relations have been applied to Gibb's monolayers in the literature, a linear relation describes the data best in our case. Note that the scatter in the data is higher at low surface coverage due to errors in the amounts spread, but the kinetic analysis is weighted on the data at higher surface coverage so this uncertainty is not particularly concerning.

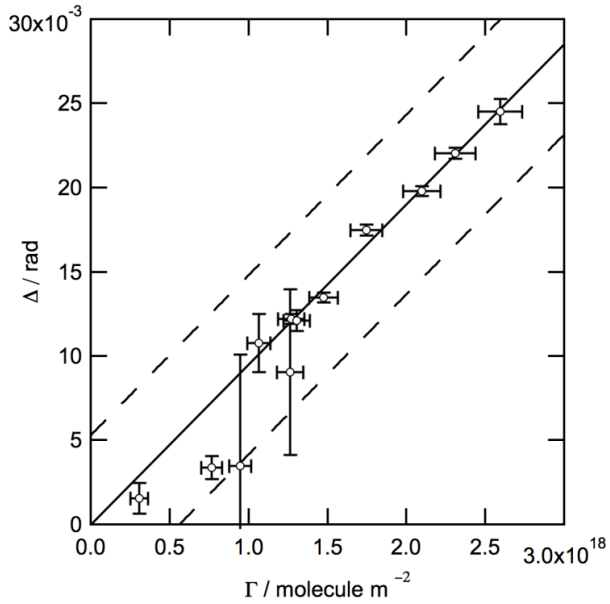

Figure S3: Calibration plot of Δ with respect to Γ for different amounts of dMO spread at the air–water interface. Error bars represent the associated uncertainties at one standard deviation. A linear fit through the origin is displayed as solid line. Dashed lines represent the 95% prediction bands.

6. Brewster angle microscopy imaging of monolayers

Brewster angle microscopy (BAM) was used to characterize the lateral morphology of the organic monolayers employed in this study. A Nanofilm EP3 instrument was used in the Partnership for Soft Condensed Matter (Grenoble, France). The short focal distance required for the measurements meant that we did not manage to use the technique with the gas-tight set-up of the miniaturised reaction chamber. Nevertheless, we did examine the lateral morphology of the starting materials using a larger open trough. Figure S4 (a) a shows a BAM image of a monolayer of hMO at 3 mN m^{-1}: the image is featureless to within the resolution of the measurement, and the layer is therefore assumed to isotropic on the micrometre scale. The highest pressure reached for a monolayer of hMO upon compression in our work is 16 mN m^{-1}, and Figure S4 (b) shows a corresponding BAM image. The presence of white spots indicates that a phase transition has taken place at the surface and that the monolayer is laterally heterogeneous. It would be useful to extend this approach in the future to the analysis of material remaining after the oxidation process has completed**.**

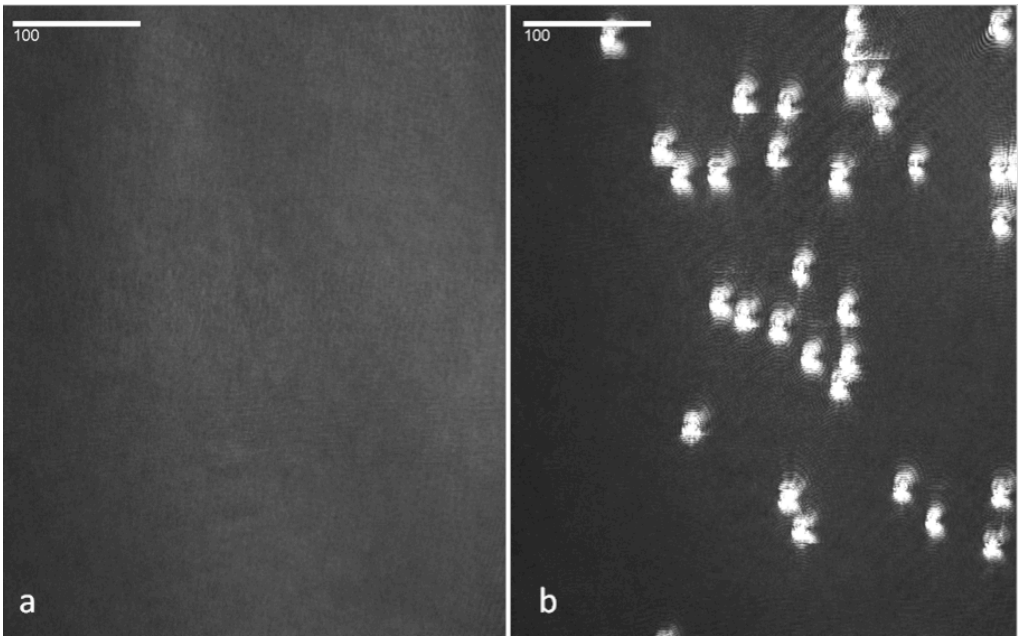

Figure S4: Brewster angle microscopy images of hMO at 25 °C on a pure water subphase recorded at two surface pressures: (a) 3 mN m^{-1} and (b) 16 mN m^{-1}. The white bars correspond to 100 μm.

7. Kinetic analysis

The surface excess values for the kinetic reactions that were calculated using eq. 3 were plotted as a function of time, and then they were fitted to obtain a rate coefficient, *k*. The fitting function used is based on the reaction of methyl oleate (MO) below.[7]

$$MO + O_3 \rightarrow \text{products} \qquad \text{(R1)}$$

$$-\frac{d[\Gamma_{MO}]}{dt} = k[\Gamma_{MO}][O_3]_{chamber} \qquad (5)$$

The concentration of ozone during the reaction was not constant owing to the gas volume above the Langmuir trough and the mixing of the added ozone. On the assumption that the chamber acted as a well stirred reactor with a constant and matched input and output volume flux, the concentration of ozone in the chamber, $[O_3]_{chamber}$, may be calculated as:

$$[O_3]_{chamber} = [O_3]_{in}\left(1 - e^{-\frac{\text{flow}}{\text{volume}}t}\right) \qquad (6).$$

Eq. 6 takes into account that the concentration of ozone needs a finite time to go from zero to the concentration of the input stream. Characteristic mixing times were ~ 10 s. As a result of the substitution of eq. 6 in eq. 5 and the integration of the differential eq. 5, we obtained the fitting function:

$$\Gamma(t) = \Gamma_0 e^{\left\{-k_1\left[t - \frac{\text{volume}}{\text{flow}}\left(1 - e^{-\frac{\text{flow}}{\text{volume}}t}\right)\right]\right\}} \qquad (7)$$

where k_1 is the first order coefficient with $k_1 = k[O_3]_s$. $[O_3]_s$ (in molecule cm^{-2}) is the concentration of ozone that dissolves into the organic layer at the air–water interface corresponding to $[O_3]_{in}$ (in molecule cm^{-3}) in the gas phase. It is calculated assuming that the surface concentration is constant in time and is equal to Henry's Law solubility:[15]

$$[O_3]_s = k_H \delta [O_3]_{in} \qquad (8)$$

where k_H is Henry's law constant for ozone (480 mol m^{-3} atm^{-1} which is an estimate taken from Smith *et al.*, 2002[15] based on measured solubilities[16,17] for O_3 in a range of organic solvents) and δ is the initial surface layer thickness (2 nm). The thickness was chosen to be consistent with previous work,[7,18] and was validated by neutron reflectometry. (The basic assumption is that O_3 from the gas-phase replenishes the surface faster than the rate at which it reacts with the organic film.)

Eq. 7 was used as fitting function for the surface excess decays through a weighted least-squares procedure. Once we determined all the values of k_1 corresponding to the O_3 surface concentrations employed in the experiments, a second-order plot was generated (k_1 *vs* $[O_3]_s$) and an orthogonal distance regression fit weighted by the uncertainties both in k_1 and $[O_3]_s$ was applied to determine *k*.

References

1. Hayter, J. B., Highfield, R. R., Pullman, B. J., Thomas, R. K., McMullen, A. I., Penfold, J. Critical reflection of neutrons. a new technique for investigating interfacial phenomena. J. Chem. Soc., Faraday Trans. 1981, 1 77, 1437–1448.

2. Lu, J., Thomas, R., Penfold, J. Surfactant layers at the air/water interface: structure and composition. Adv. Colloid Interface Sci. 2000, 84, 143–304.

3. LAMP, the Large Array Manipulation Program. http://www.ill.eu/data_treat/lamp/thelamp-book/

4. Nelson, A. Co-refinement of multiple-contrast neutron/X-ray reflectivity data using MOTOFIT. J. Appl. Cryst. 2006, 39, 273–276.

5. Armen, R. S., Uitto, O. D. & Feller, S. E. Phospholipid Component Volumes: Determination and Application to Bilayer Structure Calculations. Biophys. J. 1998, 75, 734–744.

6. Schwartz, D. K. *et al.* Thermal diffuse x-ray-scattering studies of the water--vapor interface. Phys. Rev. A 1990, 41, 5687–5690.

7. Pfrang, C., Sebastiani, F., Lucas, C.O.M., King, M.D., Hoare, I.D., Chang, D., Campbell, R.A. Ozonolysis of methyl oleate monolayers at the air–water interface: oxidation kinetics, reaction products and atmospheric implications. Phys. Chem. Chem. Phys. 2014, 16, 13220–13228.

8. Azzam, R. M. A. Bashara N. M., 1997. Ellipsometry and polarised light. North-Holland Publishing Company.

9. Day, J. P. R., Bain, C. D. Ellipsometric study of depletion at oil–water interfaces. Phys. Rev. E 2007, 76, 41601.

10. Noskov, B. A., Grigoriev, D. O., Lin, S.-Y., Loglio, G., Miller, R. Dynamic surface properties of polyelectrolyte/surfactant adsorption films at the air/water interface: Poly(diallyldimethylammonium chloride) and sodium dodecylsulfate. Langmuir 2007, 23, 9641–9651.

11. Asnacios, A., Klitzing, R., Langevin, D. Mixed monolayers of polyelectrolytes and surfactants at the air–water interface. Colloid Surf. A 2000, 167, 189–197.

12. Tonigold, K., Varga, I., Nylander, T., Campbell, R. A. Effects of aggregates on mixed adsorption layers of poly(ethylene imine) and sodium dodecyl sulfate at the air/liquid interface. Langmuir 2009, 25, 4036–4046.

13. Angus-Smyth, A., Bain, C. D., Varga, I., Campbell, R. A. Effects of bulk aggregation on PEI/SDS monolayers at the dynamic air/liquid interface: depletion due to precipitation versus enrichment by a convection/spreading mechanism. Soft Matter 2013, 26, 6103–6117.

14. Manning-Benson, S., Bain, C. D., Darton, R. C. Measurement of dynamic interfacial properties in an overflowing cylinder by ellipsometry. J. Colloid Interface Sci. 1997, 189, 109–116.

15. Smith, G. D., Woods, E., DeForest, C. L., Baer, T. and Miller, R. E. Reactive Uptake of Ozone by Oleic Acid Aerosol Particles: Application of Single-Particle Mass Spectrometry to Heterogeneous Reaction Kinetics. J. Phys. Chem. A 2002, 106, 8085–8095.

16. Razumovskii, S. D.; Zaikov, G. E. *Bull. Acad. Sci. USSR, Div. Geologic* 1971, 616–620.

17. Tarunin, B. I.; Perepletchikov, M. L.; Aleksandrov, Y. A. *Z.* Obsch. Khim. (English) 1982, 52, 419–422.

18. King, M. D., Rennie, A. R., Thompson, K. C., Fisher, F. N., Dong, C. C., Thomas, R. K., Pfrang, C. and Hughes, A. V. Oxidation of oleic acid at the air–water interface and its potential effects on cloud critical supersaturations. Phys. Chem. Chem. Phys. 2009, 11, 7699–7707.